A Human-Inspired Hybrid Control Approach to Bipedal Robotic Walking ⋆

Ryan W. Sinnet * **Matthew J. Powell** * **Rajiv P. Shah** * **Aaron D. Ames** *

* *Texas A&M University, Department of Mechanical Engineering, 3123 TAMU, College Station, TX 77843-3123*
e-mail: {rsinnet,mjpowell,rps2125,aames}@tamu.edu

Abstract: A human-inspired method for achieving bipedal robotic walking is proposed in which a hybrid model of a human is used in conjunction with experimental walking data to obtain a multi-domain hybrid system. Walking data were collected for nine test subjects; these data are analyzed in terms of the kinematics of walking. In bipedal walking, certain points on the body are constrained for various intervals throughout the gait; this phenomenon is used to formally break the gait into walking phases. The results indicate that all of the nine subjects had the same breakdown with similar times spent in each phase; in other words, this specific breakdown likely represents a *canonical human model*. Using this canonical breakdown, a controller is designed for a robotic model which mimics human kinematics behaviors by tracking functions of the kinematics—this controller is applied in simulation, resulting in stable walking which is remarkably humanlike in nature.

Keywords: Robotics; Robot kinematics; Robot control; Nonlinear control; Hybrid models

1. INTRODUCTION

Bipedal robotic walking has been well-studied for over three decades—an uncountable number of models have been studied with an almost endless combination of control laws applied in an attempt to achieve stable walking. Yet true humanlike robotic walking has been noticeably absent in the majority of research on the topic. This is likely a ramification of control design processes which lack proper consideration of human locomotion. To achieve anthropomorphic walking, it seems only reasonable to study human walking patterns and create a hybrid model based on the results of such a study. Indeed, human walking has been studied (see Zatsiorsky [1997], Sutherland et al. [2005]) and hybrid models have been created (see Grizzle et al. [2001], Sinnet and Ames [2009]); however, only recently have these endeavors been combined in an effort to create human-inspired bipedal robotic walking (see Srinivasan et al. [2008]). This paper, therefore, attempts to reconcile these ideas and obtain robotic walking as graceful as a human gait.

Researchers in biomechanics generally study forces and dynamics (see Seireg and Arvikar [1975], Winter [1990]); specifically, forces and loading have been studied at the foot (see Au et al. [2006], Rodgers [1988]) and at the hip (see Bergmann et al. [1993], Heller et al. [2001]). Force plates and force loading models allow researchers to estimate musculoskeletal forces and ground reaction forces (see Scott and Winter [1993]); these estimates are used with either forward-dynamic models (see Anderson and Pandy [2001], Neptune et al. [2001], Pandy and Berme [1988]) or inverse-dynamic models (see Glitsch and Baumann [1997], Siegler and Liu [1997]).

To model bipedal walking in this paper, we will first introduce hybrid systems—these are dynamical systems which combine both continuous dynamics as in traditional dynamical systems and discrete dynamics resulting from impacts—and constraints, which are imposed on the system to model phenomena such as ground contact. We will show how constraints can be used to develop a four domain breakdown for a hybrid model (four domain models with different domain structures have been considered, see Braun and Goldfarb [2009]); then we will combine this domain breakdown with the Lagrangian of a bipedal robot to construct a hybrid system.

Using this formalism, we examine data from a given walking gait. We will describe an experiment in which human walking data were collected for nine human subjects and how these data are used to develop a domain breakdown. We consider various constraints on the data and fit "simple" mathematical functions, e.g., a Gaussian, to these constraints. The result will be a set of fitted functions with coefficients of correlation near unity that accurately represents a human gait. We will then describe a robotic model with mass and length parameters derived from anthropometry of a chosen test subject. Using the "human" functions, we describe a control scheme which tracks the human functions and results in stable humanlike walking on the robotic model.

2. HYBRID SYSTEMS AND CONSTRAINTS

Bipedal robotic walking exhibits both discrete and continuous behavior—it is, therefore, natural to model bipedal robots as hybrid systems. A walking gait will be shown to consist of multiple domains—on each domain, the system evolves in a continuous fashion according to a dynamic model derived from a Lagrangian modeling the mechanical system on that domain. This dynamic model will depend upon which points on the robot are in contact with the ground. At a certain point in each domain, i.e. when the contact points change, the model will discretely change to another phase of walking with a different dynamic model and different control. This

⋆ R. W. Sinnet is an NSF Graduate Research Fellow. This work is supported by NSF grant CNS-0953823 and NHARP award 00512-0184-2009.

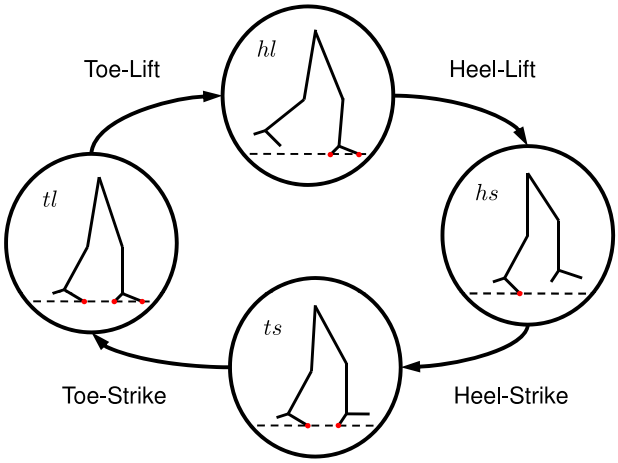

Fig. 1. An example of a *domain breakdown*, i.e., the discrete phases of a walking gait with a specific temporal ordering. The red dots indicate the constraints enforced in each discrete phase of walking.

combination of continuous and discrete phenomena constitutes a hybrid system.

This section formally introduces hybrid systems and discusses how the dynamic model of a robot together with a temporal ordering of discrete events, i.e., change in contact points, completely determines the hybrid model of a system. More specifically, to model bipedal robots, one need only consider a Lagrangian and domain breakdown.

2.1 Formal Definition of Hybrid Systems

Hybrid systems or *systems with impulse effects* (see Morris and Grizzle [2005]) have been studied extensively in a wide variety of contexts and have been used to model a wide range of bipedal robotic systems (see Grizzle et al. [2010]). This section introduces a definition of hybrid systems applicable to bipedal walking. Steady state bipedal walking is naturally periodic, motivating the use of multi-domain hybrid systems with a temporal ordering of events, i.e., hybrid systems in which the domain graph is a *directed cycle*.

Definition 1. A *directed cycle* is a graph $\Gamma = (V, E)$, with V a set of vertices and E a set of edges, [1] where

$$V = \{v_1, v_2, \ldots, v_p\}, \quad (1)$$
$$E = \{e_1 = \{v_1, v_2\}, e_2 = \{v_2, v_3\}, \ldots, e_p = \{v_p, v_1\}\},$$

with p the number of discrete domains in the hybrid model. This is illustrated in the following example:

Example 2. The domain breakdown pictured in Fig. 1 has an underlying graph which is a directed cycle; the graph is given by $\Gamma_u = (V_u, E_u)$. There are four vertices and four edges with

$$V_u = \{ts, tl, hl, hs\},$$
$$E_u = \{\{ts, tl\}, \{tl, hl\}, \{hl, hs\}, \{hs, ts\}\}.$$

Using this notion of a directed cycle, the formulation of hybrid systems which is of interest in this paper can now be introduced:

Definition 3. A *hybrid control system in a cycle* is a tuple,

$$\mathscr{HC} = (\Gamma, \mathcal{D}, U, S, \Delta, FG),$$

where

- $\Gamma = (V, E)$ is a *directed cycle*
- $\mathcal{D} = \{\mathcal{D}_v\}_{v \in V}$ is a set of *domains* with $\mathcal{D}_v \subseteq \mathcal{X}_v \times U_v$ a smooth submanifold, where $\mathcal{X}_v$ represents the state space,
- $U = \{U_v\}_{v \in V}$, with $U_v \subseteq \mathbb{R}^{m_v}$, is a set of admissible controls,
- $S = \{S_e\}_{e \in E}$ is a set of *guards* or *switching surfaces* with $S_e \subseteq D_{\mathrm{sor}(e)}$,
- $\Delta = \{\Delta_e\}_{e \in E}$ is a set of *reset maps* with $\Delta_e : \mathbb{R}^{n_{\mathrm{sor}(e)}} \to \mathbb{R}^{n_{\mathrm{tar}(e)}}$ a smooth map,
- $FG = \{(f_v, g_v)\}_{v \in E}$, where (f_v, g_v) is a *control system* on D_v, i.e., $\dot{x} = f_v(x) + g_v(x)u$ for $x \in D_v$ and $u \in U_v$.

A *hybrid system* is a hybrid control system where $U_v = \emptyset$ for all $v \in V$, i.e., where feedback controllers have been applied. In this case, we write:

$$\mathscr{H} = (\Gamma, \mathcal{D}, S, \Delta, F),$$

where $F = \{f_v\}_{v \in E}$, with f_v is a (possibly non-autonomous) *dynamical system* on $\mathcal{D}_v$, i.e., $\dot{x} = f_v(x, t)$.

2.2 Obtaining Hybrid Systems from Constraints

The remainder of this section is devoted to discussing how a Lagrangian for a biped, together with a domain breakdown (which determines the constraints at each vertex of the associated cycle), allows one to explicitly construct a hybrid model. Many details are outlined due to space constraints, but more detail can be found in Grizzle et al. [2010].

General Setup. We begin by constructing a Lagrangian for a robot in either two or three dimensions—the discussions in this paper apply to either case—in a general position, i.e., no assumptions on ground contact, and then enforce ground contact through constraints as dictated by the domain graph.

Lagrangians. Following the presentation in Grizzle et al. [2010], let R_0 be a fixed inertial or world frame and let R_b be a reference frame attached to the body of the biped with position $p_b \in \mathbb{R}^3$ and orientation $\phi_b \in SO(3)$. [2] Given a configuration space for the biped, $\mathcal{Q}_s$, i.e., a choice of body or shape coordinates for the robot—typically, $q_s \in \mathcal{Q}_s$ is a collection of relative angles between each successive link of the robot with respect to some base configuration—the *generalized* coordinates of the robot are found by combining the coordinates of the body-fixed frame, R_b, with the shape coordinates, q_s, viz.

$$q = (p_b, \phi_b, q_s) \in \mathcal{Q} = \mathbb{R}^3 \times SO(3) \times \mathcal{Q}_s,$$

with $\mathcal{Q}$ the generalized configuration space.

The Lagrangian of a bipedal robot, $\mathcal{L} : T\mathcal{Q} \to \mathbb{R}$, can be stated in terms of the kinetic energy, $T : T\mathcal{Q} \to \mathbb{R}$, and the potential energy, $V : \mathcal{Q} \to \mathbb{R}$, as:

$$\mathcal{L}(q, \dot{q}) = T(q, \dot{q}) - V(q),$$

with $T\mathcal{Q}$ the tangent bundle of $\mathcal{Q}$. The Euler-Lagrange equation allows one to find the dynaimc model, which, for robotic systems (cf. Murray et al. [1994]), takes the form

$$D(q)\ddot{q} + H(q, \dot{q}) = B(q)u, \quad (2)$$

where $D(q)$, the inertia matrix, and $B(q)$, the torque distribution matrix, depend on q, u is a vector of applied torques, and

$$H(q, \dot{q}) = C(q, \dot{q})\dot{q} + G(q)$$

contains terms resulting from the Coriolis effect and gravity.

[1] We denote the source and target of an edge $e \in E$ by $\mathrm{sor}(e)$ and $\mathrm{tar}(e)$, respectively.

[2] SO(n) represents the special orthogonal group in n dimensions (cf. Conway et al. [1986]).

Constraints. The dynamic model depends on which constraints are enforced on a given domain or transition—in other words, which contact points are in contact with the ground. Formally, we define the *contact set* $\mathcal{C} = \{c_1, c_2, \ldots, c_k\}$ with each c_i representing a specific type of contact possible in the biped. Assuming that foot contact is restricted to the toe or heel edge, there are four contact points of interest: $\mathcal{C} = \{c_{\text{sh}}, c_{\text{st}}, c_{\text{nsh}}, c_{\text{nst}}\}$, where these constraints represent the stance heel, stance toe, non-stance heel, and non-stance toe, respectively.[3] We specialize to this set of contact points in this paper for reasons that become clear after our data analysis.

Contact points introduce *holonomic constraints*, η_c for $c \in \mathcal{C}$, on the system; this vector must be held constant for the contact point to be maintained. To construct these constraints, consider a reference frame, R_c, at the contact point c such that the axis of rotation about this point (either the heel or toe) is along the y-axis. Let $R_0^c : \mathcal{Q} \to SO(3)$ be a transformation between R_0 and R_c, $p_c : \mathcal{Q} \to \mathbb{R}^3$ be the Cartesian position of the frame, and $v_c(q, \dot{q}) = \dot{p}_c(q, \dot{q})$ be the velocity of the frame. The body-fixed angular velocity (see Jazar [2007]) is then given by

$$\Omega_c(q, \dot{q}) = \left(R_0^c(q)\right)^T \frac{\partial R_0^c(q)}{\partial q}\dot{q} = \begin{bmatrix} 0 & -\omega_c^z & \omega_c^y \\ \omega_c^z & 0 & -\omega_c^x \\ -\omega_c^y & \omega_c^x & 0 \end{bmatrix}.$$

Note that this skew-symmetric matrix $\Omega_c(q, \dot{q})$ is dual to the angular velocity vector $\omega_c = (\omega_c^x, \omega_c^y, \omega_c^z)$.[4] Then, define

$$\eta_c(q, \dot{q}) = \begin{bmatrix} v_c(q, \dot{q}) \\ \omega_c^x(q, \dot{q}) \\ \omega_c^z(q, \dot{q}) \end{bmatrix} = J_c(q)\,\dot{q},$$

where $J_c(q)$ is a Jacobian matrix. In the case of 2D bipeds, as in this paper, the treatment is exactly the same but $\eta_c(q, \dot{q}) = (v_c^x(q, \dot{q}), v_c^z(q, \dot{q}))$. By choosing the given holonomic constraint, one can impose the condition $\eta_c(q, \dot{q}) = \text{constant}$, which fixes the contact point to the ground but allows rotation about the heel or toe edge. It is useful to express the collection of all holonomic constraints in a matrix, $\eta(q, \dot{q}) \in \mathbb{R}^{20\times 4}$, as

$$\eta(q, \dot{q}) = \text{blockdiag}\left(\eta_{sh}, \eta_{st}, \eta_{nsh}, \eta_{nst}\right),$$

where we have suppressed dependence on q and $\dot{q}$.

Another class of constraints that is important is the class of *unilateral constraints*, $h_c(q)$ for $c \in \mathcal{C}$, since they dictate the set of admissible configurations of the system. Assuming that the walking is on flat ground, these constraints represent the height of a contact point above the ground, i.e., $h_c(q) = p_c^z(q)$, and can be put in the form of a matrix $h(q) \in \mathbb{R}^{4\times 4}$ in the same manner as holonomic constraints: $h(q) = \text{diag}\left(h_{sh}, h_{st}, h_{nsh}, h_{nst}\right)$.

Domain Breakdowns. A *domain breakdown* is a directed cycle with a specific choice of contact points on every vertex. Formally, we assign to each vertex a binary vector describing which contact points are enforced on that domain.

Definition 4. Let $\mathcal{C} = \{c_1, c_2, \ldots, c_k\}$ be a set of contact points and Γ be a directed cycle. A *domain breakdown* is a function $\mathcal{B} : V \to \mathbb{Z}_2^k$ such that $B_i(v) = 1$ if c_i is constrainted on v and $B_i(v) = 0$ otherwise.

Example 5. Using the domain breakdown in Fig. 1 with graph Γ_u from Example 2 and $C = \{c_{\text{sh}}, c_{\text{st}}, c_{\text{nsh}}, c_{\text{nst}}\}$, the breakdown is formally given by $\mathcal{B}_u : V_u \to \mathbb{Z}_2^4$ where

$$\mathcal{B}_u(ts) = [\,1\ 0\ 0\ 1\,]^T,\ \ \mathcal{B}_u(tl) = [\,1\ 1\ 0\ 1\,]^T,$$
$$\mathcal{B}_u(hl) = [\,1\ 1\ 0\ 0\,]^T,\ \mathcal{B}_u(hs) = [\,0\ 1\ 0\ 0\,]^T.$$

2.3 Hybrid System Construction

In this section, we demonstrate that, given a Lagrangian, a directed cycle, and a domain breakdown, a hybrid model can be explicitly constructed. Since the Lagrangian is intrinsic to the robot being considered, a domain breakdown alone dictates the mathematical model of the biped.

Continuous Dynamics. We explicitly construct the control system $\dot{x} = f_v(x) + g_v(x)u$ through the constraints imposed on each domain by the domain breakdown. For domain $v \in V$, the holonomic constraints are $\eta_v(q, \dot{q}) = \eta(q, \dot{q})\mathcal{B}(v)$. The Jacobian is found by differentiating $\eta_v(q, \dot{q})$ viz.

$$J_v(q) = \text{Basis}\left(\text{RowSp}\left(\frac{\partial \eta_v(q, \dot{q})}{\partial q}\right)\right). \tag{3}$$

By considering a basis for the row space of the Jacobian, redundant constraints are removed so $J_v(q)$ has full row rank. Using (3), one can write the *constrained dynamic model* as

$$D(q)\ddot{q} + H(q, \dot{q}) = B(q)u + J_v(q)F_v, \tag{4}$$

where D, H and B are as in (2) and F_v is *wrench* containing forces and moments expressed in the reference frame R_c (see Murray et al. [1994]). The wrench $F_v : T\mathcal{Q} \times U_v$ is found by differentiating the constraint $J_v(q)\dot{q} = \text{constant}$,

$$J_v(q)\ddot{q} + \frac{\partial}{\partial q}\left(\frac{\partial J_v(q)}{\partial q}\dot{q}\right)\dot{q} = 0,$$

and combining this with (4) to obtain

$$F_v(q, \dot{q}, u) = -\big(J_v(q)D^{-1}(q)J_v^T(q)\big)^{-1}\Big(\dot{J}_v(q, \dot{q})\,\dot{q} + J_v(q)D^{-1}(q)\big(B(q)u - H(q, \dot{q})\big)\Big). \tag{5}$$

This wrench is commonly referred to as a Lagrange multiplier (see Murray et al. [1994]). Combining (4) and (5) allows one to eliminate $F_v(q, \dot{q}, u)$ and obtain the fields associated to the control system $\dot{x} = f_v(x) + g_v(x)u$. For $x = (q, \dot{q})$,

$$f_v(q, \dot{q}) = \begin{bmatrix} \dot{q} \\ D^{-1}(q)\Big(\big(J_v^T(q)\Xi(q)J_v(q)D^{-1}(q) - I\big)H(q, \dot{q}) - J_v^T(q)\Xi(q)\dot{J}_v^T(q, \dot{q})\dot{q}\Big) \end{bmatrix}, \tag{6}$$

$$g_v(q) = \begin{bmatrix} \mathbf{0} \\ D^{-1}(q)\big(I - J_v^T(q)\Xi(q)J_v(q)D^{-1}(q)\big)B(q) \end{bmatrix},$$

where, for simplicity, $\Xi(q) := \big(J_v(q)D^{-1}(q)J_v^T(q)\big)^{-1}$.

Discrete Dynamics. We now construct the domains, guards, and reset maps for a hybrid system using the domain breakdown. Given a vertex $v \in V$, the domain is the set of admissible configurations of the system factoring in both friction, ground torque limitations, and a unilateral constraint. Specifically, from the wrench $F_v(q, \dot{q}, u)$, one can ensure that the foot does not slip by considering inequalities on friction which can be stated:

$$\mu_v(q)F_v(q, \dot{q}, u) \geq 0, \tag{7}$$

with $\mu_v(q)$ a matrix of friction parameters and constants defining the geometry of the foot (see Grizzle et al. [2010] for more details). It was shown in Vukobratović et al. [1990], Chevallereau et al. [2009] that the moment produced by the ground is limited; this limitation has the form:

[3] Sometimes the non-stance heel and toe are referred to as the swing heel and toe. We prefer the notation non-stance due to the existence of double support phases where there is no "swinging" behavior. In this case, the stance leg is the leg holding most of the weight of the biped.

[4] By an abuse of notation, we have suppressed the dependence of ω_c on $(q, \dot{q})$.

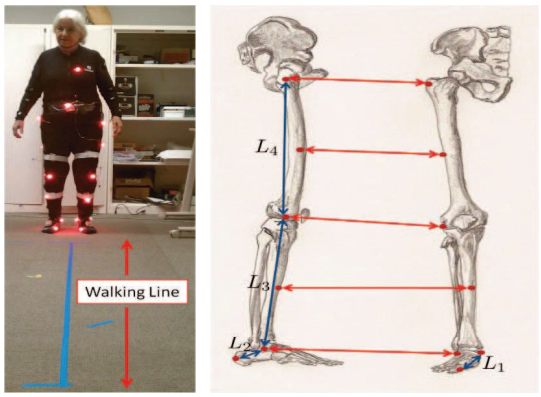

Fig. 2. Experimental setup (left) and sensor placement (right). Each subject wore a suit with affixed sensors. Sensors were placed at the joints as illustrated with the red dots on the right lateral and anterior aspects of the legs. The same sensors from different views are connected with red arrows (right) and the labeled blue arrows are used to illustrate the diversity of subjects in Table 1.

$$\nu_v(q)F_v(q,\dot{q},u) \geq 0, \tag{8}$$

where $\nu_v(q)$ depends on the physical parameters and state of the system. Combining (7) and (8) with a unilateral constraint $h_v(q) = h(q)\mathcal{B}(v)$ (if present) yields

$$A_v(q,\dot{q},u) = \begin{bmatrix} \mu_v(q)F_v(q,\dot{q},u) \\ \nu_v(q)F_v(q,\dot{q},u) \\ h_v(q) \end{bmatrix} \geq 0. \tag{9}$$

Using (9) allows one to express the domain of admissibility:

$$D_v = \{(q,\dot{q},u) \in T\mathcal{Q} \times U_v : A_v(q,\dot{q},u) \geq 0\}. \tag{10}$$

The guard is just the boundary of this domain with the additional assumption that set of admissible configurations is decreasing, i.e., the vector field is pointed outside of the domain, or, for an edge $e = (v, v') \in E$,

$$S_e = \Big\{(q,\dot{q},u) \in TQ \times U_v : A_v(q,\dot{q},u) = 0 \text{ and } \dot{A}_v(q,\dot{q},u) \leq 0\Big\}.$$

The impact model is derived by considering the constraints on the target domain. For an edge $e = (q, q') \in E$, the post-impact velocity $\dot{q}^+$ is given in terms of the pre-impact velocity $\dot{q}^-$:

$$\dot{q}^+ = P_e(q,\dot{q}^-) = (I - D^{-1}J_{q'}^T(J_{q'}D^{-1}J_{q'})^{-1}J_{q'})\dot{q}^-$$

with I the identity matrix. In order to obtain periodic behavior, the "left" and "right" leg must be "swapped" at one of the transitions; this trick is common throughout the literature (see Grizzle et al. [2001]). This is done with a coordinate transformation $\mathcal{R}$ switching the role of the left and right legs, i.e., a state relabeling procedure; using this, the reset map is written

$$\Delta_e(q,\dot{q}) = \begin{bmatrix} \mathcal{R}_e & \mathbf{0} \\ \mathbf{0} & \mathcal{R}_e \end{bmatrix} \begin{bmatrix} q \\ P_e(q,\dot{q}) \end{bmatrix}.$$

The end result is that given a domain breakdown and a bipedal robot, the hybrid model is completely determined. The goal of this paper is to determine the domain breakdowns that humans use and this section demonstrated the importance of the domain breakdown in determining the unique model of a system.

3. DOMAIN BREAKDOWN FROM HUMAN DATA

We now determine the domain breakdown for nine test subjects. We begin by discussing the experiment; see Fig. 2. We then present a method for determining the times during which the constraint for a given contact point is enforced through a method that fits a simple function to the motion of the contact point when it is unconstrained; when it is constrained, it is constant. This procedure yields a temporal ordering of events which leads to a domain breakdown. The result is a single *universal* domain breakdown for all of the subjects, which is used to construct the hybrid model studied in this paper.

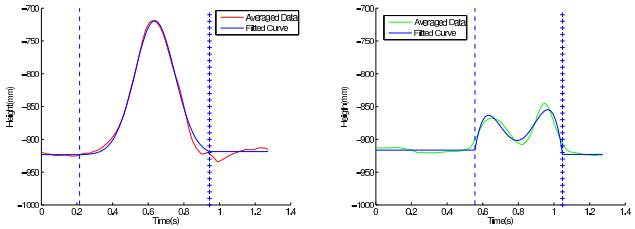

(a) Heel height and fit. (b) Toe height and fit.

Fig. 3. The data for the heel and toe heights with the fittings of a constant, Gaussian, and constant for the heel and a constant, fourth order polynomial, and constant for the toe.

Walking Experiment. Data were collected on nine subjects using the PhaseSpace Motion Capture System, which computes the 3D position of 19 LED sensors at 480 frames per second using 12 cameras at a one millimeter level of accuracy. The cameras were calibrated prior to the experiment and were placed to observe a space of size five by five by five meters. Eight LED sensors were placed on each leg at the joints and the heel and toe, one on the sternum, one on the back behind the sternum, and one on the umbilicus. Each trial required a subject to walk three meters along a line on the floor. Each subject performed 12 trials, which constituted a single experiment. Three female and six male subjects were tested; the variation in subjects is best seen in Table 1. The data for each individual are rotated so the walking occurs in the x direction and, for each subject, the 12 walking trials are averaged, resulting in a single trajectory for each constraint for at least two steps (one step per leg); see Fig. 3. The data are available online; see URL:Supplementary Material.

Function Fitting. The domain breakdown for each subject is obtained by determining the times when the enforced contact points change or the *event times*. Instead of using force sensors, we assume a given contact point is fixed when constrained and look for a simple function that it follows when unconstrained.

Table 1. Table describing each of the subjects. The subject number is in the left column and the L_1, L_2, L_3, L_4 measurements correspond to the lengths in Fig. 2. The measurements in column 4 are in kilograms and in columns 5–9 are centimeters.

	Sex	Age	Weight	Height	L_1	L_2	L_3	L_4
1	M	30	90.7	184	14.5	8.50	43.0	44.0
2	F	19	53.5	164	15.0	8.00	41.0	44.0
3	M	17	83.9	189	16.5	8.00	45.5	55.5
4	M	22	90.7	170	14.5	9.00	43.0	39.0
5	M	30	68.9	170	15.0	8.00	43.0	43.0
6	M	29	59.8	161	14.0	8.50	37.0	40.0
7	M	26	58.9	164	14.0	9.00	39.0	41.0
8	F	77	63.5	163	14.0	8.00	40.0	42.0
9	F	23	47.6	165	15.0	8.00	45.0	43.0

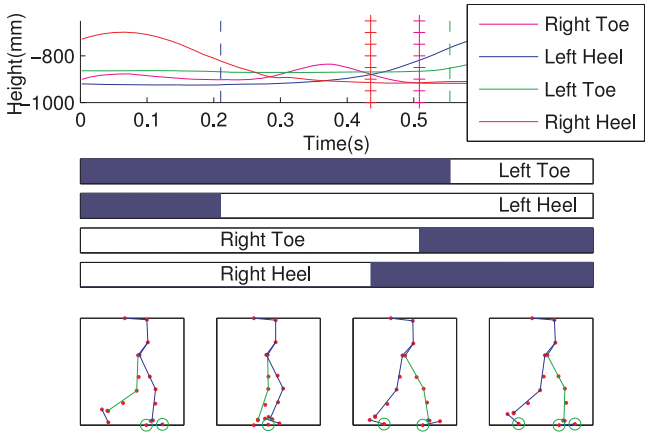

Fig. 4. An overview of the domain breakdown procedure. Top: heights of the toes and heels over one step along with the lift and strike time for each constraint (vertical lines). Middle: active constraints. Bottom: domain breakdown with enforced constraints drawn as green circles.

To formalize this procedure, given a set of contact points $\mathcal{C}$, let $s_c(t, a_c)$ be a *human* function that a contact point $c \in \mathcal{C}$ follows when not in contact with the ground; here $a_c \in R^{n_c}$ are function parameters. Denote the indexed human data for c by $y_c[k]$, with $\tau[k]$ the time corresponding to datum $y_c[k]$ for discrete index variable $k \in \{1, \dots, T\}$. When the contact point is constrained, it is constant, and when it is unconstrained, it follows $s_c(t, a_c)$. Therefore, we consider the function

$$f_c(t) = f_c(t, k_c^\ell, k_c^s, a_c) = \begin{cases} s_c(\tau[k_c^\ell], a_c), & t \leq \tau[k_c^\ell], \\ s_c(t, a_c), & \tau[k_c^\ell] < t < \tau[k_c^s], \\ s_c(\tau[k_c^s], a_c), & \tau[k_c^s] \leq t, \end{cases}$$

where $\tau[k_c^\ell], \tau[k_c^s] \in \{\tau[k]\}_{k=1}^T$ are the event times indicating when c becomes unconstrained (lift) and constrained (strike), respectively. We assume $k_c^\ell < k_c^s$; if this is not true, then f_c would consist of the human function, followed by a constant, followed by the human function. [5] To calculate the event times, we solve the following optimization problem

$$\min_{k_c^\ell, k_c^s \in \{1,\dots,T\}} \min_{a_c \in \mathbb{R}^{n_c}} \sum_{k=1}^{T} \left(f_c(t, k_c^\ell, k_c^s, a_c) - y_c(t) \right)^2$$

for each $c \in \mathcal{C}$. Assuming the foot is rigid and flat, there are four relevant constraints: one at the heel and one at the toe for both the left and right feet. Since each constraint has a lift and strike time, we have eight domains in one whole step. However, in robotics, we typically consider stance and non-stance legs; without the distinction of left and right, the model is reduced to four domains. Doing so allows one to exploit the symmetry inherent in bipedal walking to simplfy controller design.

To illustrate this procedure, consider the averaged data for the heel and toe in Fig. 3. The height of the heel appears to follow a constant, followed by a Gaussian, followed by a constant; therefore, we claim that the human function which the heel follows when unconstrained is a Gaussian. Similarly, the toe height appears to follow a constant, followed by a fourth order polynomial, followed by a constant. We fit the averaged heel and toe data to these functions using the described procedure.

[5] After the construction of the f_c functions in this paper, the optimization parameters are supressed, but it is assumed they have been determined.

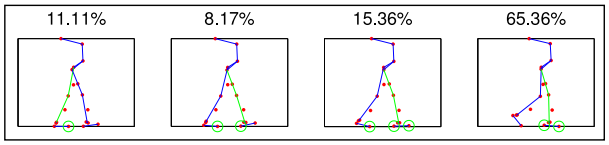

Fig. 5. The domain breakdown for subject 4 and the times spent in each domain. Each tile shows the configuration at the beginning of the domain and the contact points enforced.

The results are shown in Fig. 3 with the transition points $\tau[k_c^\ell]$ and $\tau[k_c^s]$ indicated by vertical lines. The fits quite accurately represent the data; indeed, the coefficients of correlation for the heel and toe are 0.9968 and 0.9699, respectively.

For the contact point $c \in \mathcal{C}$, we determine the lift and strike times, $\tau[k_c^\ell]$ and $\tau[k_c^s]$ for $c \in \mathcal{C} = \{c_1, c_2, c_3, c_4\} = \{c_{\mathrm{lh}}, c_{\mathrm{lt}}, c_{\mathrm{rh}}, c_{\mathrm{rt}}\}$, over the time interval of the averaged data, $\left[\tau[1], \tau[T]\right]$. Since the data comprise at least two steps (one step with each leg), there are multiple lift and strike times in one period. Denote by $\mathcal{J}_c \subset \left[\tau[1], \tau[T]\right]$ the period where c is constrained, i.e., $t \in \mathcal{J}_c$ if $f_c(t) = \text{constant}$ with f_c the fitting function for the contact point $c \in \mathcal{C}$; these intervals are shown in blue in Fig. 4 over the course of one step (not the entire data period) in the case of $\mathcal{C} = \{c_{\mathrm{lh}}, c_{\mathrm{lt}}, c_{\mathrm{rh}}, c_{\mathrm{rt}}\}$. Analogous to the definition of a domain breakdown (Definition 4), we define a binary vector, $b(t) \in \mathbb{Z}_2^{|\mathcal{C}|}$, with $|\mathcal{C}|$ representing the cardinality of $\mathcal{C}$, encoding which contact points are constrained at any given time by letting $b_i(t) = 1$ if $t \in \mathcal{J}_{c_i}$ for $i \in \{1, \dots, |\mathcal{C}|\}$.

Determining the Domain Breakdown. First, define the directed cycle Γ (if it exists, which is not guaranteed). Then, $b(t)$ takes on only a finite number of values, say, N values; denote these values by $d[n]$ for $n \in \{1, \dots, N\}$. For the walking to be periodic, there must exist a positive $p \in \mathbb{Z}$ satisfying

$$d[n + p] = \begin{bmatrix} \mathbf{0} & I \\ I & \mathbf{0} \end{bmatrix} d[n] \tag{11}$$

for $n \in \{1, \dots, p\}$ with I the identity matrix and $\mathbf{0}, I \in \mathbb{R}^{|\mathcal{C}|/2 \times |\mathcal{C}|/2}$. If the data constitute multiple steps, there will be more than one possible value for p; in this case, the proper value of p is the smallest of these values as this represents one step. The matrix that is premultiplied by $d[n]$ serves the purpose of reordering the right leg and left leg. If this p can be found, periodic walking over the course of two steps has been discovered in the data with the behavior of the left leg mirroring the behavior of the right leg. In this case, one constructs a directed cycle with p domains (as in (1)) and this is the graph Γ. The corresponding domain breakdown $\mathcal{B}$ is given by $\mathcal{B}(v_n) = d[n]$ for $n \in \{1, \dots, p\}$. The application of this procedure to subject 4 can be seen in Fig. 4.

Results. We perform the process outlined for the set of contact points $\mathcal{C} = \{c_{\mathrm{sh}}, c_{\mathrm{st}}, c_{\mathrm{nsh}}, c_{\mathrm{nst}}\}$ on the nine subjects. The end result showed each subject had the same *universal* domain breakdown; this can be seen in Fig. 1. In the context of this paper, a single subject (subject 4) was chosen for study based upon the completeness of the sensor data; the domain breakdown and the time spent in each domain are shown in Fig. 5.

4. HUMAN-INSPIRED CONTROLLER DESIGN

The goal of this section is to find functions that are "canonical" to human walking, i.e., functions that seem intrinsic to walking. These functions are used to generate a controller using feedback

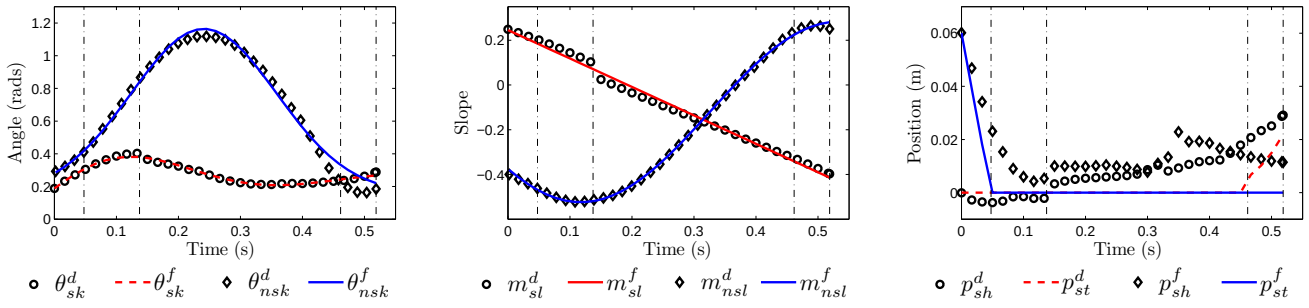

(a) Angular constraints (b) Slope constraints (c) Height constraints

Fig. 6. Human data over the course of one step with one leg and the fitted functions. The plots start at the beginning of domain ts, with vertical lines indicating transitions between domains. The plotted variables are shown in Fig. 8(b).

linearization for a robot with anthropomorphic measurements. This technique is shown to result in stable walking despite the differences between the robotic and human locomotive systems.

4.1 "Canonical" Walking Functions.

Instead of tracking human trajectories, we seek functions which have simple representations (e.g., heel and toe height), yet describe fundamental behaviors of human walking. From the perspective of control, the functions must not conflict with the constraints of the system on each domain as dictated by the enforcement of robot-ground contact points.

With these goals in mind, we consider the walking data from subject 4 obtained through the process outlined in Sec. 3. Inspection of various kinematic relationships indicates that functions describing the behavior of the torso, leg angles (see Fig. 8(b), knee angles, and the heel and toe heights seem to encode the most fundamental behaviors associated to human walking. The humanlike behavior of these different functions through the course of the walking gait of a human can be seen in Fig. 6, where the data begin at the start of domain ts.

Knee. Inspecting the behavior of the human knee (see Fig. 6(a)), we find that the knee angle appears to follow a Gaussian when swinging (the non-stance leg) and a second order system response when supporting the weight of the person (the stance leg). We thus fit the following functions for the angles of the stance and non-stance knees:

$$y_{d,sk\angle} = -A_{2,1}\,\frac{\cos(A_{2,2}\,t) - A_{2,3}\sin(A_{2,2}\,t)}{\exp(A_{2,4}\,t)} + A_{2,5},$$

$$y_{d,nsk\angle} = A_{5,1}\,\exp\left(\frac{-(t-A_{5,2})^2}{2(A_{5,3})^2}\right) + A_{5,4}.$$

In other words, the stance leg is essentially a spring-damper system responding to the impulse of the body weight of the person as he or she puts his or her weight on that leg whereas the non-stance leg is free to swing.

Leg. For the leg slopes as in Fig. 6(b), i.e., the slope of the line between the ankle and the hip (see Fig. 8(b)), the stance leg slope appears to move forward linearly in time and the non-stance leg slope follows a sinusoid:

$$y_{d,slm} = A_{3,1}\,t + A_{3,2},$$
$$y_{d,nsl} = A_{6,1}\,\sin(A_{6,2}\,t + A_{6,3}) + A_{6,4}.$$

Intuitively, this means that the stance leg moves forward monotonically forcing the motion of the biped forward, while the non-stance leg swings freely much like the non-stance knee.

Foot. The behaviors of the heel and toe are more complicated (see Fig. 6(c)): the functions describing these heights are quite simple (see Fig. 3), yet it is generally not be feasible to follow these exact functions as doing so would create conflicts with the holonomic constraints enforced on certain domains causing singularities in the controller. Therefore, we segment the behavior of the feet based upon the domain breakdown of the human subject. In particular, in domain ts, the goal of walking is to cause the toe to strike the ground. We find the height of the toe nearly follows a linear function,

$$y_{d,sth} = A_{7,1}\,t + A_{7,2},$$

after which point the toe is fixed to the ground. In a similar light, in domain hs, the goal is to effect heel lift. As such, the non-stance heel lifts according to a Gaussian:

$$y_{d,shh} = A_{1,1}\,e^{\frac{-(t-A_{1,2})^2}{2(A_{1,3})^2}} + A_{1,4}.$$

Torso and Ankle. It is desirable to keep the torso upright. We find from the data that the angle of the torso with respect to the world frame follows a sinusoid with small amplitude; we approximate this with a constant:

$$y_{d,T\angle} = A_{4,1}.$$

Finally, when the leg is swinging, we approximate the behavior of the ankle angle with a constant:

$$y_{d,nsa\angle} = A_{8,1}.$$

Fitting. The paramaters of the human functions are found by minimizing the error between the human data and the corresponding functions; see Fig. 6. The correlation coefficients for the fits can be found in Table 2; in all cases (with the exceptions of the torso and ankle) the fits are very good.

4.2 Robotic Hybrid Model & Controllers

We now consider the robot shown in Fig. 8(a) and attempt to design controllers using the human functions.

Robotic Model. It was shown in Sec. 2 that one can explicitly construct a hybrid control system for a set of contact points and a domain breakdown. Using the procedure from Sec. 3, we obtain the domain breakdown, $\mathcal{B}_u$, representing human walking (see Example 5), defined on the cycle $\Gamma_u = (\mathcal{Q}_u, V_u)$ (given in Example 2). Using the construction in Sec. 2, we obtain:

$$\mathscr{HC} = (\Gamma_u, \mathcal{D}, U, S, \Delta, FG).$$

The configuration space, $\mathcal{Q}_r$, is chosen to be the relative angles between successive links. The parameters of the system are

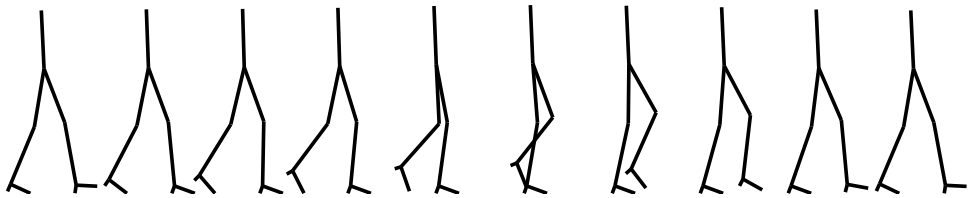

Fig. 7. Snapshots of simulated walking gait.

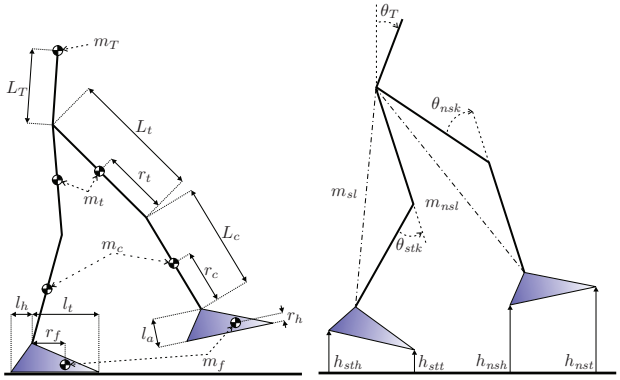

(a) Robot configuration (b) Robot constraints

Fig. 8. (a) The configuration of the robot. (b) The configuration-based variables of the human functions.

unknowns; these are obtained from the data for subject 4 in Table 1. The point masses (see Fig. 8(a)) are estimated using a standard mass distribution (see Winter [1990]).

Controller Design. Our goal now is to design a controller to track the human functions given in Sec. 4.1. We will perform this tracking using feedback linearization (see Sastry [1999]).

We begin by considering a control system of the form (f_v, g_v), with $v \in V_u$, as given in (6) for a single domain. Let $y_v^a(q)$ represent the vector of "actual" outputs on the system (e.g., the height of the stance heel)—these can be found from the forward kinematics—and let $y_v^d(t)$ represent the vector of "desired" output functions we wish to track consisting of combinations of the human functions. Let $n = \dim(\mathcal{Q})$ and let m be the number of constraints imposed on a given domain. A control law which drives $y_v^a(q(t)) \to y_v^d(t)$ as $t \to \infty$ is the following:

$$u(q,\dot{q},t) = -\mathcal{A}_v^{-1}(q,\dot{q})\big(L_{f_v}L_{f_v}y_v^a(q) - \ddot{y}_v^d(t) + 2\epsilon(L_{f_v}y_v^a(q) - \dot{y}_v^d(t)) + \epsilon^2(y_v^a(q) - y_v^d(t))\big),$$

with $\mathcal{A}_v(q,\dot{q})$ the decoupling matrix given by

$$\mathcal{A}_v(q,\dot{q}) = L_{g_v}L_{f_v}y_v^a(q),$$

Applying this control law yields the closed-loop system

$$f_{cl,v}(q,\dot{q},t) = f_v(q,\dot{q}) + g_v(q)u(q,\dot{q},t).$$

The vector y_v^a consists of the robotic constraints in Fig. 8(b) computed from the forward kinematics. The specific choice of functions is shown in Table 2, with black dots indicating which functions are used on which domain; this choice is based on the discussion in Sec. 4.1. Applying these controllers to each domain results in the non-autonomous hybrid system

$$\mathscr{H} = (\Gamma_u, \mathcal{D}, S, \Delta, F).$$

5. SIMULATIONS AND CONCLUDING REMARKS

Simulation of $\mathscr{H}$ shows that the biped exhibits stable walking. Stability is verified by finding a fixed point and applying the Poincaré map technique. We use the physical model parameters found at URL:Supplementary Material and the control gain $\varepsilon = 100$. The resulting fixed point is then:

$$q_s^* = (-0.3969, 0.2431, 0.2133, -0.4159, 0.3314, 0.0525),$$
$$\dot{q}_s^* = (-1.2331, 0.4907, 0.7423, 0.1118, -2.7557, 14.0877)$$

which is on the guard of domain hl. The presence of this fixed point verifies that a walking gait exists.

In the context of bipedal walking, a stable limit cycle or an exponentially stable periodic orbit implies stable walking. We would, therefore, like to show that our system has a stable limit cycle. We will do this by examining the Jacobian of the Poincaré map linearized about the fixed point $(q^*, \dot{q}^*)$ (cf. Parker and Chua [1989]). This Poincaré map will be stable if all the eigenvalues of the Jacobian have magnitude below unity. Then, stability of the Poincaré map implies stability of the limit cycle. The Jacobian can be approximated by perturbing about the fixed point with respect to the coordinates q and $\dot{q}$. A numerical approximation yields eigenvalues with magnitudes:

$$|\lambda| \in \{1.1 \times 10^{-1}, 1.1 \times 10^{-4}, 4.0 \times 10^{-6}, \mathbf{0}_9\}.$$

where eigenvalues with magnitude less than 10^{-6} are approximated as the zero vector $\mathbf{0}_9$. We start on the guard corresponding to heel lift so $(q_0, \dot{q}_0) = (0, 0)$, with q_0 the angle between the stance foot and ground, and thus these eigenvalues are not present. If we were to find the fixed point in a domain where these coordinates were allowed to be nonzero, we would find an extra two eigenvalues, but these would have magnitude zero (cf. Wendel and Ames [2010]).

Since the eigenvalues have magnitude below unity, we have a locally exponentially stable periodic orbit. These phase portraits shown in Fig. 9 are continuous so we have a periodic orbit. Snapshots of the walking gait are shown in Fig. 7. These simulation results imply that, through a choice of functions intrinsic to human walking, we were able to obtain surprisingly anthropomorphic walking on a bipedal robot model.

Table 2. Correlations and choice of functions on each domain.

Eq.	Constraint	r	ts	tl	hl	hs
$y_{d,shh}$	Stance heel height	0.73671				•
$y_{d,ska}$	Stance knee angle	0.99213	•	•	•	•
$y_{d,slm}$	Stance leg slope	0.99534	•	•	•	•
$y_{d,T\angle}$	Torso absolute angle	*	•	•	•	•
$y_{d,nsk\angle}$	Non-stance knee angle	0.99301	•	•	•	•
$y_{d,nsl}$	Non-stance leg slope	0.99971			•	
$y_{d,sth}$	Stance toe height	0.99971	•			
$y_{d,nsa\angle}$	Non-stance ankle angle	*			•	•

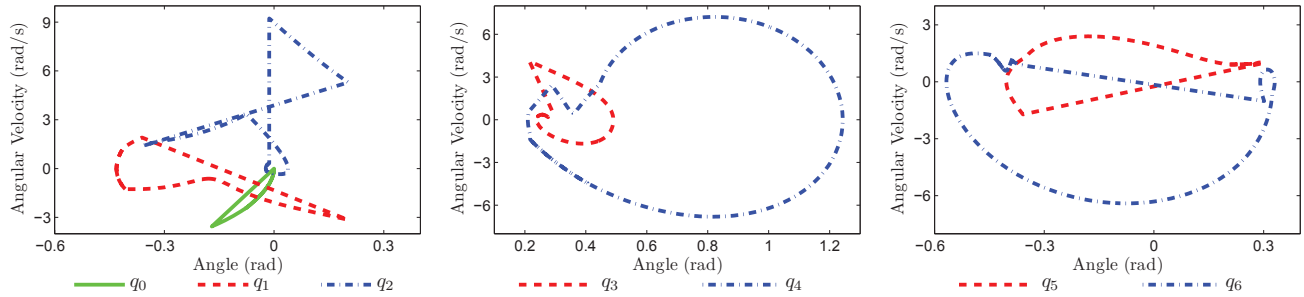

(a) Ankle angles and ground angle (b) Knee angles (c) Hip angles

Fig. 9. Phase portraits showing results from the simulation of $\mathscr{H}$. These phase portraits are closed, indicating that they represent limit cycles or periodic orbits. In the context of bipedal locomotion, this means we have stable walking.

REFERENCES

F. C. Anderson and M. G. Pandy. Dynamic optimization of human walking. *ASME J. of Biomech. Eng.*, 123(5):381–90, October 2001.

S. K. Au, P. Dilworth, and H. Herr. An ankle-foot emulation system for the study of human walking biomechanics. In *IEEE Intl. Conf. Robotics and Automation*, pages 2939–45, Orlando, May 2006.

G. Bergmann, F. Graichen, and A. Rohlmann. Hip joint loading during walking and running, measured in two patients. *J. of Biomech.*, 26(8):969–90, August 1993.

D. J. Braun and M. Goldfarb. A control approach for actuated dynamic walking in bipedal robots. *IEEE TRO*, 25(6):1292–303, December 2009.

C. Chevallereau, G. Bessonnet, G. Abba, and Y. Aoustin. *Bipedal Robots: Modeling, Design and Walking Synthesis*. Wiley-ISTE, New York, January 2009.

J. H. Conway, R. T. Curtis, S. P. Norton, R. A. Parker, and R. A. Wilson. The groups $\mathbf{GO}_n(q)$, $\mathbf{SO}_n(q)$, $\mathbf{PGO}_n(q)$, $\mathbf{PSO}_n(q)$, and $\mathbf{O}_n(q)$. In *Atlas of Finite Groups: Maximal Subgroups and Ordinary Characters for Simple Groups*, pages xi–xii, Oxford, January 1986. Clarendon Press.

U. Glitsch and W. Baumann. The three-dimensional determination of internal loads in the lower extremity. *ASME J. of Biomech. Eng.*, 30(11):1123–31, November 1997.

J. W. Grizzle, G. Abba, and F. Plestan. Asymptotically stable walking for biped robots: Analysis via systems with impulse effects. *IEEE TAC*, 46(1):51–64, January 2001.

J. W. Grizzle, C. Chevallereau, A. D. Ames, and R. W. Sinnet. 3D bipedal robotic walking: models, feedback control, and open problems. In *IFAC Symposium on Nonlinear Control Systems*, Bologna, September 2010.

M. O. Heller, G. Bergmann, G. Deuretzbacher, L. Dürselen, M. Pohl, L. Claes, N. P. Haas, and G. N. Duda. Musculoskeletal loading conditions at the hip during walking and stair climbing. *J. of Biomech.*, 34(1):883–93, July 2001.

R. N. Jazar. *Theory of Applied Robotics: Kinematics, Dynamics, and Control*. Springer, 1st edition, February 2007.

B. Morris and J. W. Grizzle. A restricted Poincaré map for determining exponentially stable periodic orbits in systems with impulse effects: Application to bipedal robots. In *44th IEEE Conf. on Decision and Control and European Control Conf.*, Sevilla, December 2005.

R. M. Murray, Zexiang Li, and S. S. Sastry. *A Mathematical Introduction to Robotic Manipulation*. CRC Press, Boca Raton, March 1994.

R. R. Neptune, S. A. Kautz, and F. E. Zajac. Contributions of the individual ankle plantar flexors to support, forward progression and swing initiation during walking. *J. of Biomech.*, 34(11):1387–98, November 2001.

M. G. Pandy and N. Berme. A numerical method for simulating the dynamics of human walking. *J. of Biomech.*, 21(12): 1043–51, April 1988.

T. S. Parker and L. O. Chua. *Practical numerical algorithms for chaotic systems*. Springer, New York, August 1989.

M. M. Rodgers. Dynamic biomechanics of the normal foot and ankle during walking and running. *Physical Therapy*, 68(12): 1822–30, December 1988.

S. S. Sastry. *Nonlinear Systems: Analysis, Stability and Control*. Springer, New York, June 1999.

S. H. Scott and D. A. Winter. Biomechanical model of the human foot: Kinematics and kinetics during the stance phase of walking. *J. of Biomech.*, 26(9):1091–104, September 1993.

A. Seireg and R. J. Arvikar. The prediction of muscular load sharing and joint forces in the lower extremities during walking. *J. of Biomech.*, 8:89–102, March 1975.

S. Siegler and W. Liu. *Three-Dimensional Analysis of Human Locomotion*, chapter Inverse Dynamics in Human Locomotion, pages 191–209. John Wiley & Sons, New York, 1st edition, 1997.

R. W. Sinnet and A. D. Ames. 2D bipedal walking with knees and feet: A hybrid control approach. In *Joint 48th IEEE Conf. on Decision and Control and 28th Chinese Control Conf.*, pages 3200–7, Shanghai, December 2009.

S. Srinivasan, I. A. Raptis, and E. R. Westervelt. Low-dimensional sagittal plane model of normal human walking. *ASME J. of Biomech. Eng.*, 130(5), October 2008.

D. H. Sutherland, K. R. Kaufman, and J. R. Moitoza. *Human Walking*, chapter Kinematics of Normal Human Walking, pages 23–44. Lippincott Williams & Wilkins, Baltimore, 3rd edition, December 2005.

URL:Supplementary Material, 2011. `http://www1.mengr.tamu.edu/aames/ifac_2011_spsa_01/`.

M. Vukobratović, B. Borovac, D. Surla, and D. Stokic. *Biped Locomotion*. Springer-Verlag, Berlin, March 1990.

E. D. B. Wendel and A. D. Ames. Rank properties of Poincaré maps for hybrid systems with applications to bipedal walking. In *Hybrid Systems: Computation and Control*, pages 151–60, Stockholm, April 2010.

D. A. Winter. *Biomechanics and Motor Control of Human Movement*. Wiley-Interscience, New York, 2nd edition, May 1990.

V. M. Zatsiorsky. *Kinematics of Human Motion*. Human Kinetics, Champaign, 1st edition, September 1997.